NOAA Technical Memorandum ERL WPL-228

RADAR IMAGING OF THE SEA SURFACE USING DIFFERENT POLARIZATIONS: COMPARISON BETWEEN THEORY AND EXPERIMENT

Valery U. Zavorotny

Wave Propagation Laboratory
Boulder, Colorado
January 1993

noaa NATIONAL OCEANIC AND ATMOSPHERIC ADMINISTRATION / Environmental Research Laboratories

NOAA Technical Memorandum ERL WPL-228

RADAR IMAGING OF THE SEA SURFACE USING DIFFERENT POLARIZATIONS: COMPARISON BETWEEN THEORY AND EXPERIMENT

Valery U. Zavorotny
Cooperative Institute for Research in Environmental Sciences
University of Colorado
Boulder, Colorado

Wave Propagation Laboratory
Boulder, Colorado
January 1993

UNITED STATES
DEPARTMENT OF COMMERCE

Barbara Hackman Franklin
Secretary

NATIONAL OCEANIC AND
ATMOSPHERIC ADMINISTRATION

John A. Knauss
Under Secretary for Oceans
and Atmosphere/Administrator

Environmental Research
Laboratories

Joseph O. Fletcher
Director

NOTICE

Mention of a commercial company or product does not constitute an endorsement by the NOAA Environmental Research Laboratories. Use of information from this publication concerning proprietary products or the tests of such products for publicity or advertising purposes is not authorized.

For sale by the National Technical Information Service, 5285 Port Royal Road
Springfield, VA 22061

CONTENTS

Radar Imaging of the Sea Surface Using Different Polarizations: Comparison Between Theory and Experiment

Valery U. Zavorotny

ABSTRACT

Recently obtained polarimetric radar images of ocean areas are considered. The first attempt to find a possible explanation for drastic differences between two different polarizations is made. At the same time a summary of the existing theoretical models for radar scattering and imaging is presented. Various theoretical approaches are examined in order to understand the origin of the polarization peculiarities. It is found that these images cannot be explained with the two-scale Bragg model. New approaches reviewed here represent only a collection of physical mechanisms that should be synthesized in a consistent way. Another, more robust theory of electromagnetic wave scattering on the real ocean surface is desirable for radar image interpretation.

1. Introduction

In recent years, a microwave radar has been successfully used to monitor ocean surface waves and, in particular to detect various kinds of surface effects, e.g., ocean ripples, currents, pollution (oil patches). Besides the undoubted success of using radar to remotely sense the ocean surface, the potentialities of that method have not yet been completely revealed. To confirm this, note a number of articles that are devoted to fundamentally new and powerful remote sensing technologies, such as real-aperture radar imaging, synthetic-aperture radar imaging, and imaging radar polarimetry (see, e.g., *Alpers et al.*,1981; *Etkin et al.*, 1991, *Zebker and Van Zyl*, 1991). These methods make it possible to obtain multipolarized radio images of the ocean surface with high spatial resolution.

The theory, which describes the radar signature as a function of polarization, dates back to the early 1950's, but it has taken the more

recent development of both real-aperture radar and synthetic-aperture radar and also the availability of high-performance computers to permit practical investigations of high-resolution, multifrequency imaging radar polarimetry. Indeed, a practical imaging radar polarimetry system requires a suitable delivery platform, calibrated transmitting and receiving equipment, computational algorithms for deriving the scattering vector coefficients, high-performance computational power, and understanding of the relationship between actual surface structure and measured polarization scattering.

The last requirement remains vital particularly for the case of ocean-surface radar polarimetry. Recent observations of Russian scientists (*Etkin et al.*, 1991; *Mityagina et al.*, 1991) reveal very important peculiarities in the real-aperture radar images obtained at two different orthogonal polarizations. The difference between microwave radar returns at orthogonal polarizations is not unexpected. Much experimental and theoretical evidence of this difference was obtained from the early days of using the radar technique (see, e.g., *Beckmann and Spizzichino*, 1963; *Scolnik*, 1968; *Barrick*, 1972). *Wright* (1966) found that the backscatter of microwave radiation (λ = 3 cm) from mechanically generated water waves of small amplitude is polarization dependent. The return for vertical polarization is greater than that for horizontal polarization, and the ratio increases with angle of incidence ϑ and the relative dielectric constant of the fluid.

Then a similar effect was found for the wind-generated sea surface, but the polarization data were characterized by more complexity and greater variability, which usually relate to the complex shape of the real sea surface and its strong dependence on environmental parameters (*Scolnik*, 1968). The composite of backscattering cross-section data for two polarizations is shown in Fig. 1. One can see that the most pronounced difference between vertical and horizontal polarization takes place for small grazing angles. This phenomenon attracted the attention of researchers, and other new details were soon obtained. For example, *Kalmykov and Pustovoytenko* (1976) observed, at grazing incidence, that a significant portion of the backscatter of horizontally polarized energy is produced by the crests of waves, while the backscatter of vertically polarized energy is more distributed over the whole wave. Some of these polarization differences can be explained using the existing theory; some of them remain without

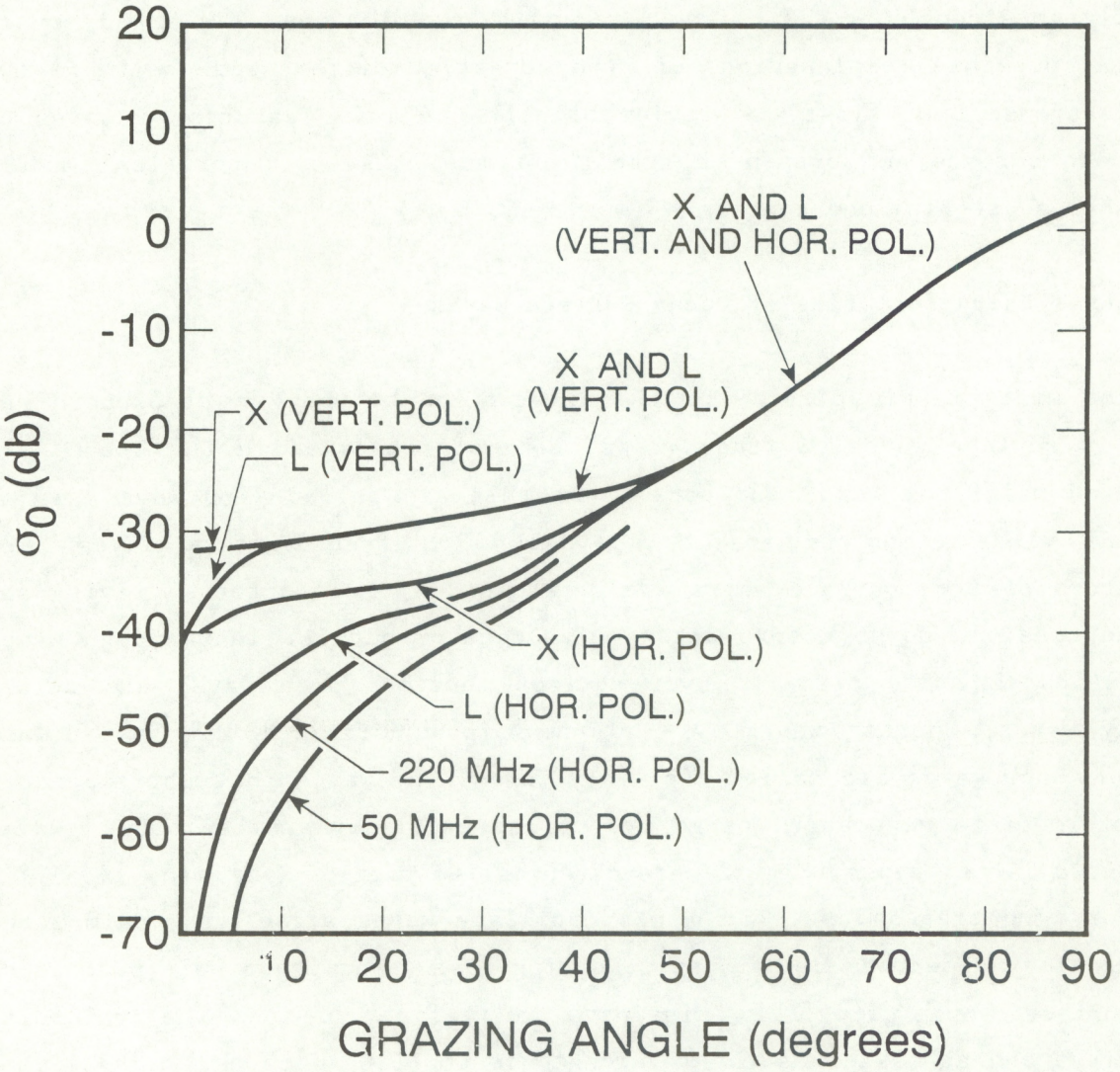

Figure 1. The composite of backscattering cross-section data for two polarizations (vertical and horizontal) for a "medium" sea (*Scolnik*, 1968).

reasonable theoretical support until now.

Below we consider unique polarimetric radar images of vast ocean areas recently obtained by *A. V. Smirnov* (private communication, 1991) and try to find a possible explanation of the drastic differences between two polarizations. But, first, we review briefly the main features of waves on the ocean surface and present a summary of the existing theoretical models for radar scattering and imaging.

2. General Characteristics of Ocean Surface Waves

The most graphic display of the interaction between an atmosphere and ocean is surface waves. Surface waves, commonly observed in the ocean, are generated mainly by wind, and because of this are called wind waves. If an external wind action is absent, we deal with free surface waves. The parameters of free surface waves are determined by two factors, gravity and surface tension. Both factors act simultaneously, but for long enough waves ($\lambda_s \geq 10$ cm) gravity prevails over surface tension. Such waves are called gravity waves. Shorter waves ($\lambda_s \leq 0.4$cm) are conditioned only by surface tension. Such waves are called capillary waves. The waves that correspond to the intermediate wavelength range are called capillary-gravity waves. Waves of the two latter types (Fig. 2) are often called ripples (*Kinsman*, 1965).

For wind speeds less than 1 m/s capillary waves arise on a calm water surface. They appear to be very swift during gusts, forming ripple patches on the surface, but they also dissipate very fast due to the molecular viscosity, and as faster as the wavelength is smaller. When the wind becomes stronger, then more large, gravity wind waves arise. In real conditions waves of various types exist simultaneously on the ocean surface, from capillary waves with wavelengths of several millimeters to gravity waves with wavelengths of several hundred meters (the latter wave is called a swell). The maximal wave height depends on the wind speed, wind duration, and fetch, the length over which the wind continues to act on the arising and propagating wave.

Wind waves on the ocean surface are random (Fig. 2). Because of this, they should be described using statistical characteristics, probability density functions for the surface elevations, correlation functions, spectra,

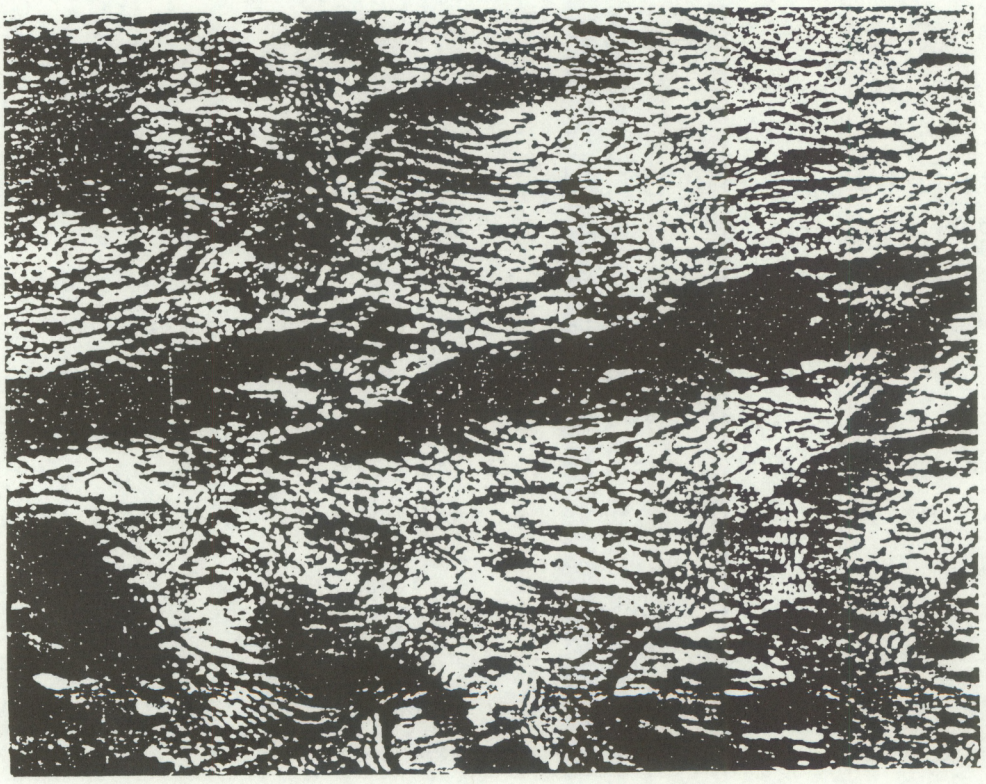

Figure 2. Capillary fine structure superimposed on larger waves, as they appear at sea (*Kinsman*, 1965).

and so forth. The most often used characteristics are the wave spectra, which determine the energy distribution over frequencies (or wavenumbers) and over propagation directions of wave harmonics of the random wave field. Wind wave spectra are rather narrow both over frequencies and over propagation directions. A bulk of the energy is concentrated in the frequency band of about one octave. The phase velocity of the energy-bearing components of the wind waves is about the mean wind velocity.

Contrary to surface ocean waves, the internal waves can arise in the ocean owing to the density stratification of water masses. If a layer of lighter water is placed above a layer of heavier water (a stable stratification), then we have an interface similar to the interface between an atmosphere and an ocean, which can also produce wave motions. Ocean water masses usually have a stable stratification, which is strongly pronounced in the so-called density step located on the lower boundary of the upper mixed layer, at a depth of about a few tens of meters. Because of this, internal waves occur everywhere at all oceanic regions.

Sometimes internal waves can reach the ocean surface and then interact with the surface waves. One possible mechanism of that interaction is the following. The internal waves generate weak horizontally nonuniform currents having convergence lines above the node of a wave at the pycnocline. If these currents are strong enough, then a noticeable modulation of the surface waves by currents is possible (Fig. 3.; *Hughes and Grant*, 1978). In the main, it is a linear kinematic effect associated with refraction of a surface wave on nonuniform currents. A more complex interaction is possible, which is linked with nonlinear energy exchange between surface and internal waves. In addition, the surface-active agents can be concentrated along the convergence lines, which may suppress the short surface waves and produce smooth surface areas, slicks, stretched along these lines. The internal wave manifestations at the ocean surface can be observed visually (Fig. 3) or using a microwave radar technique. Figure 4 is a radar image of internal waves on a background of ripple, obtained from a drifting ship (*Bravo-Zhivotovskiy et al.*, 1982).

More impressive images of various large-scale phenomena in the ocean are apparent when airborne real aperture radars and satellite SAR are used. These images give a more global view of the sea state over a large area with a relatively short time exposure and a good spatial resolution. Another

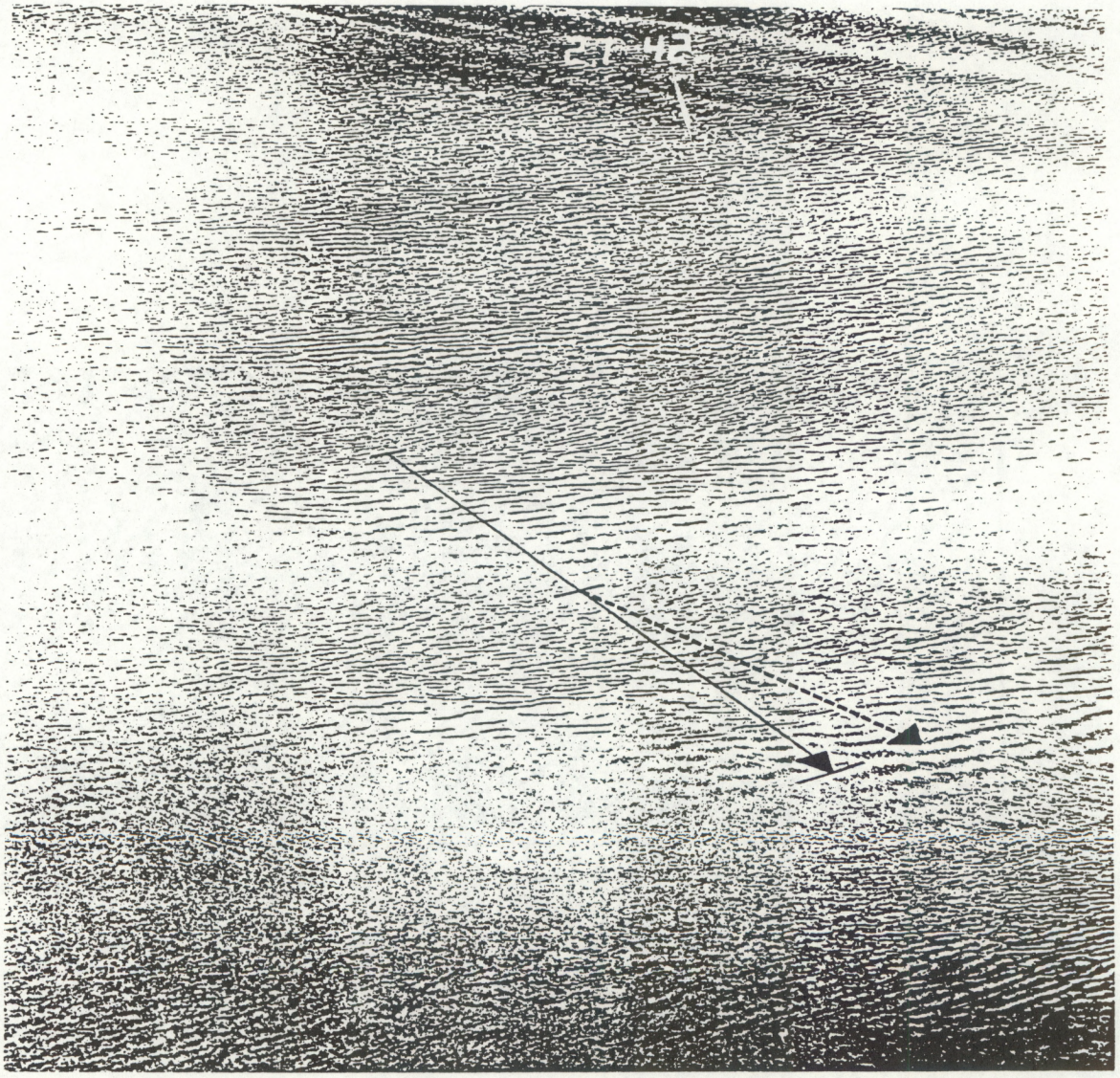

Figure 3. Aerial photograph showing the details of the surface pattern of strong surface effects. The solid arrow indicates the direction of propagation of the internal wave pattern (but not its axis of symmetry). The short bars are 50 m apart on the sea surface. The dashed arrow indicates the wind direction (*Hughes and Grant*, 1978).

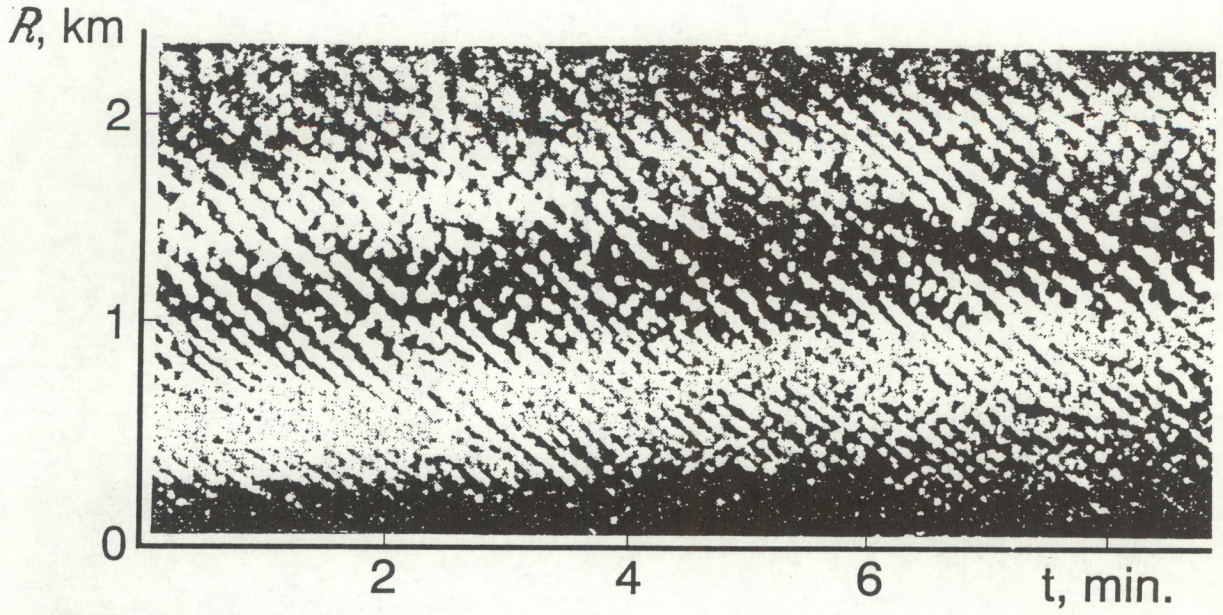

Figure 4. Radar image of internal waves on a background of ripple, obtained from a drifting research ship (*Bravo-Zhivotovskiy et al.*, 1982).

possibility for providing such images is to use imaging radar polarimetry, which can supply more valuable information about the ocean surface. However, the first results obtained in experiments with radar imaging at twopolarizations show problems related to adequate interpretation. The following section contains a description of such data.

3. Experiments with Polarization-Diverse Radar Imaging

The first simultaneous radar images at two orthogonal polarizations,shown in Fig. 5, seem to provide no surprises (*Etkin et al.*, 1991). They more or less correspond to existing theoretical predictions that characterize the radar return for the horizontal (HH) polarization as being lower by approximately 10 dB than for the vertical (VV) polarization without radically changing the spatial spectra of the images. Later we discuss this problem in more detail. But a recent experiment (*A.V. Smirnov*, private communication, 1991) reveals paradoxical behavior of similar images obtained in different conditions that cannot be explained using conventional theoretical models. In Fig. 6 we can see two radar images of the sea surface in the northwestern area of the Pacific Ocean.

The left image was obtained with horizontal polarization and the right one of the same area was obtained at the same time with vertical polarization of the transmitted and received radio waves. The images were obtained with the airborne, real-aperture radar (RAR) (also known as the side-looking radar (SLR)). The same equipment was used as in experiments by *Lavrova et al.* (1991). The wavelength used was 2.25 cm.

The geometry of the experiment is presented on Fig. 7. The speed v and the height H of the airplane Antonov-24 were 80-110 m/s and 2100-3500 m, respectively. The radar antenna had a broad beam-width in the vertical plane and a narrow beamwidth in the azimuth ($\vartheta_b = 0.2^0$). Owing to this narrow beamwidth and the corresponding pulse duration $\Delta\tau$, the linear resolution in the x and y directions on the ocean surface was ~ 30-40 m. The beam in the vertical plane was limited by incidence angles $\vartheta_1 = 55^0$ and $\vartheta_2 = 85^0$.

The rectangular frames on Figs. 6*a* and 6*b* correspond to the rectangular area on the ocean surface with dimensions ~ 12 km × 36 km. Before comparing the two images, one should take into account that the frames in Figs. 6*a* and

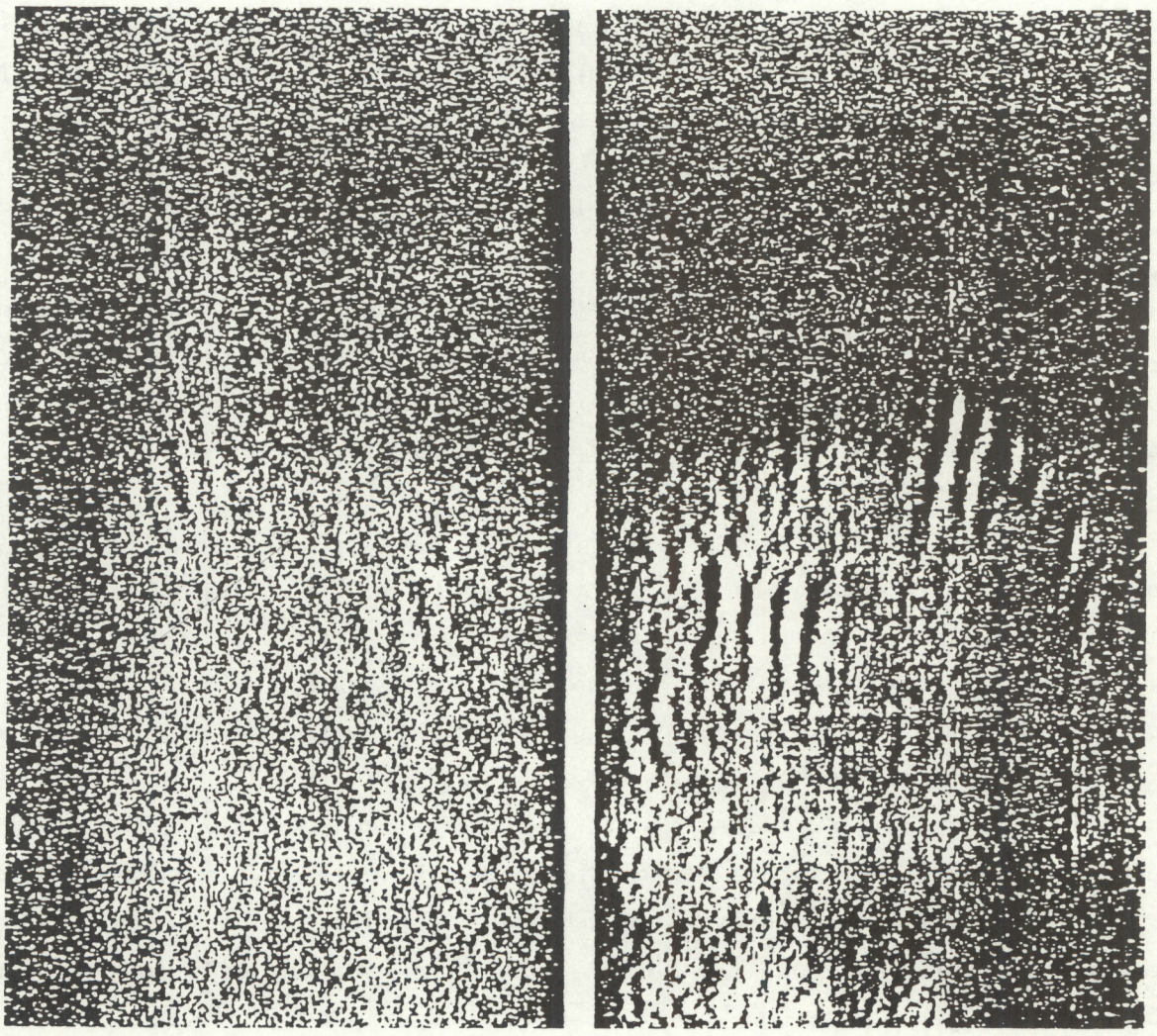

Figure 5. Radar images of sea surface manifestation of inner waves in the atmosphere: (a) *HH* polarization; (b) *VV* polarization (*Etkin et al.*, 1991).

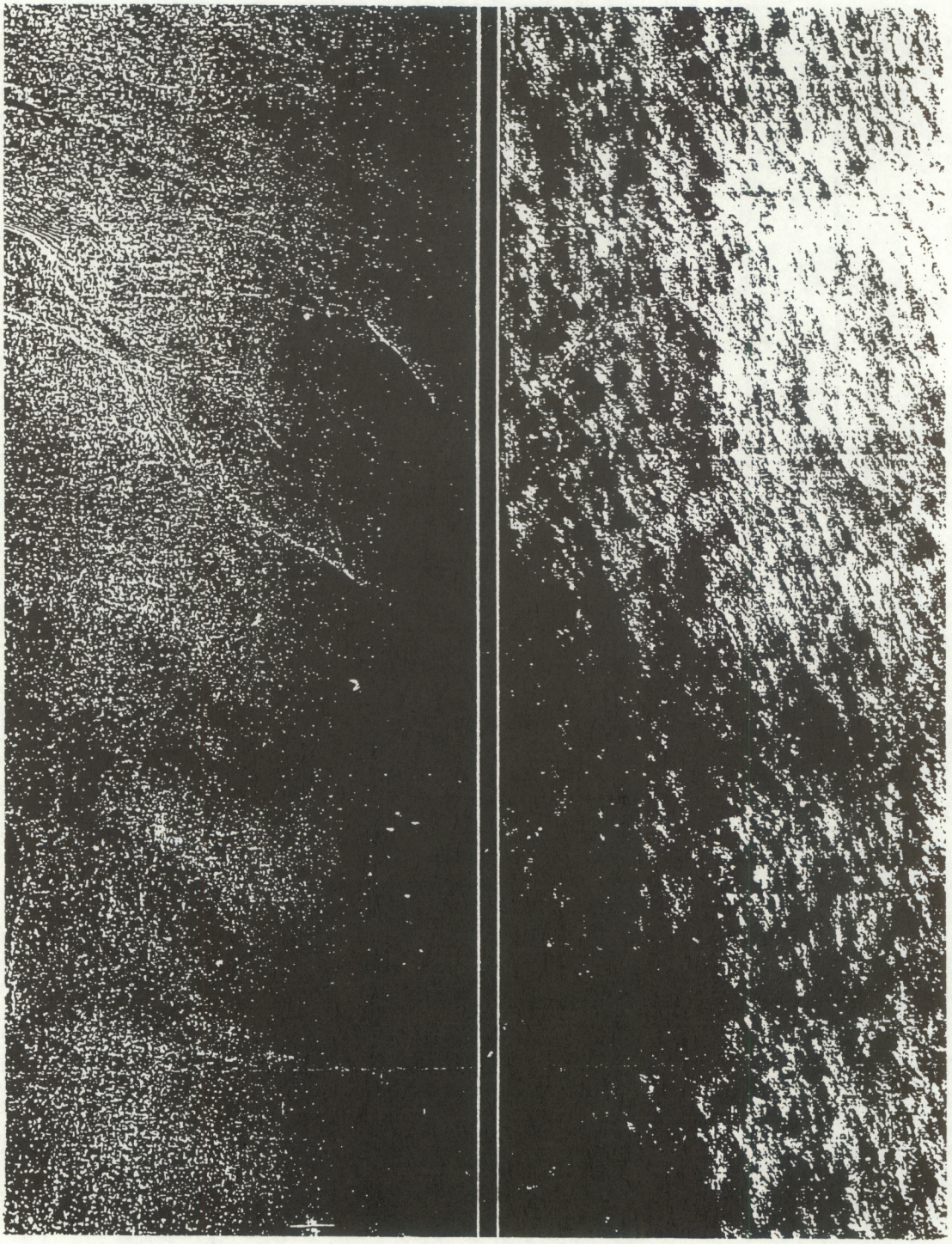

Figure 6. RAR images of the ocean surface: (a) *HH* polarization; (b) *VV* polarization (*Smirnov*, 1991).

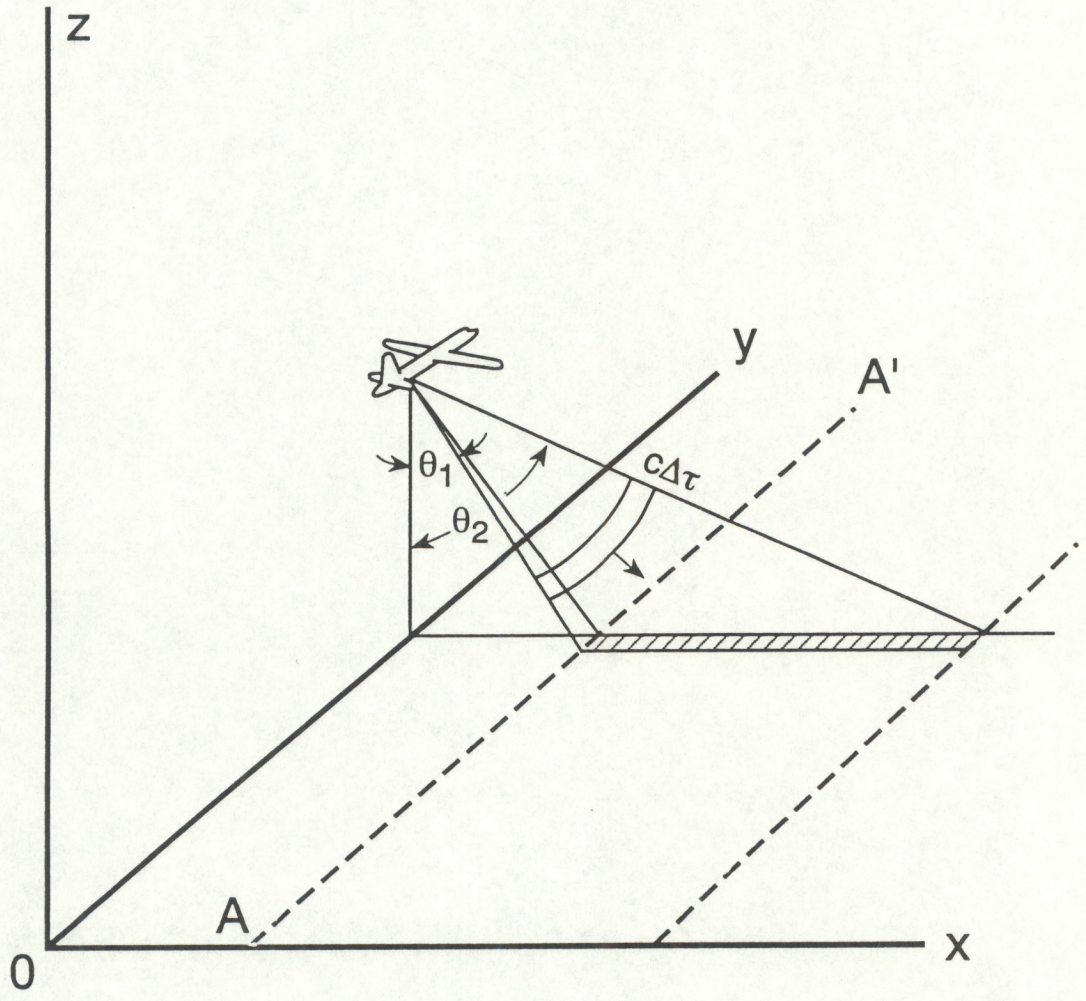

Figure 7. The geometry of the experiment.

6*b* are specularly symmetrical; i.e., the line *AA'* in Fig. 7 corresponds to the right frame edge in Fig. 6*a* and to the left frame edge in Fig. 6*b*.

The most prominent feature in the presented pictures is that the ocean image in the HH-polarization bears almost no resemblance to the one in the VV-polarization. To be exact, however, the images in Figs. 6*a* and 6*b* do have some common features. For example, we can see the quasi-periodical structure in the upper part of the frames. It seems to image the surface manifestation of internal waves. The right frame almost masks that quasi-periodical structure with the bright cell-like structure, resembling atmospheric processes near the surface, such as convection.

One important condition during this experiment was that the wind speed near the surface was pretty weak, a few meters per second. Previous experiments with two polarizations that produced no surprises were carried out under stronger wind. This fact does not allow us to consider the developed sea state, which involves breaking gravity waves, as a reasonable model for our case. Another difficulty with the interpretation of radar images from Fig. 6 is an absence of available quantitative characteristics of the images, such as spatial spectra and cross-correlation functions. Because of this the presented work is a preliminary, searching study, and all the conclusions are presumable. Below we consider various theoretical approaches in order to reach a better understanding of the origin of the polarization peculiarities.

4. The Kirchhoff Method and Perturbation Theory

The Kirchhoff method (or specular point model) is usually applied for cases of almost normal incidence to the mean surface, i.e., $\vartheta \leq 20^0$-30^0 (*Bass and Fuks*, 1979). According to this method, the main contribution to the scattering field comes from the specularly reflecting patches, having a size larger than the Fresnel scale, $(\lambda L)^{1/2}$, where L is the distance to a patch. Because of the almost normal incidence, the reflection of both the horizontally and the vertically polarized radiation should be the same. In our geometry we have $55^0 \leq \vartheta \leq 85^0$, which means that for realistic values for the slopes of the surface waves, we do not have surface patches with specular reflection; therefore the Kirchhoff method is useless for our purposes.

Perturbation scattering theory can be applied to the scattering of waves from a surface with roughness that on the scale of wavelength λ is either small and gently sloping, or smooth. *Peak* (1959) obtained a first-order backscattering cross section for a dielectric slightly rough surface for horizontal and vertical polarizations:

$$\sigma_{ij}^{(1)}(\vartheta) = 4\pi k^4 \cos^4\vartheta \left| g_{ij}^{(1)}(\vartheta) \right|^2 W(2k\sin\vartheta,\ 0), \tag{1}$$

where $W(q_x, q_y)$ is the two-dimensional wave-number spectral density of the surface roughness $\xi(\mathbf{r})$,

$$W(\mathbf{q}) = (2\pi)^{-2} \iint \langle \xi(\mathbf{r}) \xi(\mathbf{r} + \mathbf{r}') \rangle \exp(-i\mathbf{q}\mathbf{r}')\, d\mathbf{r}', \tag{2}$$

$\mathbf{r} = \{x, y\}$, $\mathbf{q} = \{q_x, q_y\}$ is the wave vector of the surface roughness, and the incident wave vector is in the x-z plane (z being the vertical direction and x, y the horizontal coordinates). The scattering geometry is shown in Fig. 8. The indices ij in Eq. (1) denote the polarization state of the incident wave and the backscattered wave, respectively. Functions $g_{ij}^{(1)}(\vartheta)$ are the first-order scattering coefficients. One can see from Eq. (1) that the Bragg resonance condition takes place; i.e., for a backscatterer, only water waves of number $2k\sin\vartheta$ traveling parallel to the line of sight contribute. For horizontal polarization

$$g_{HH}^{(1)}(\vartheta) = (\epsilon - 1)/[\cos\vartheta + (\epsilon - \sin^2\vartheta)^{1/2}]^2, \tag{3}$$

and for vertical polarization

$$g_{VV}^{(1)}(\vartheta) = \frac{(\epsilon - 1)[\epsilon(1 + \sin^2\vartheta) - \sin^2\vartheta]}{[\epsilon\cos\vartheta + (\epsilon - \sin^2\vartheta)^{1/2}]^2}, \tag{4}$$

where ϵ is the relative dielectric constant of the sea water. For free space, $\epsilon = 1$; for $\lambda = 3$ cm (X band), $\epsilon = 48 - 35i$; for $\lambda = 24$ cm (L band), $\epsilon = 73 - 85i$. At HF ($f \sim 3$-30 MHz, $\lambda \sim 100$-10 m) and lower frequencies

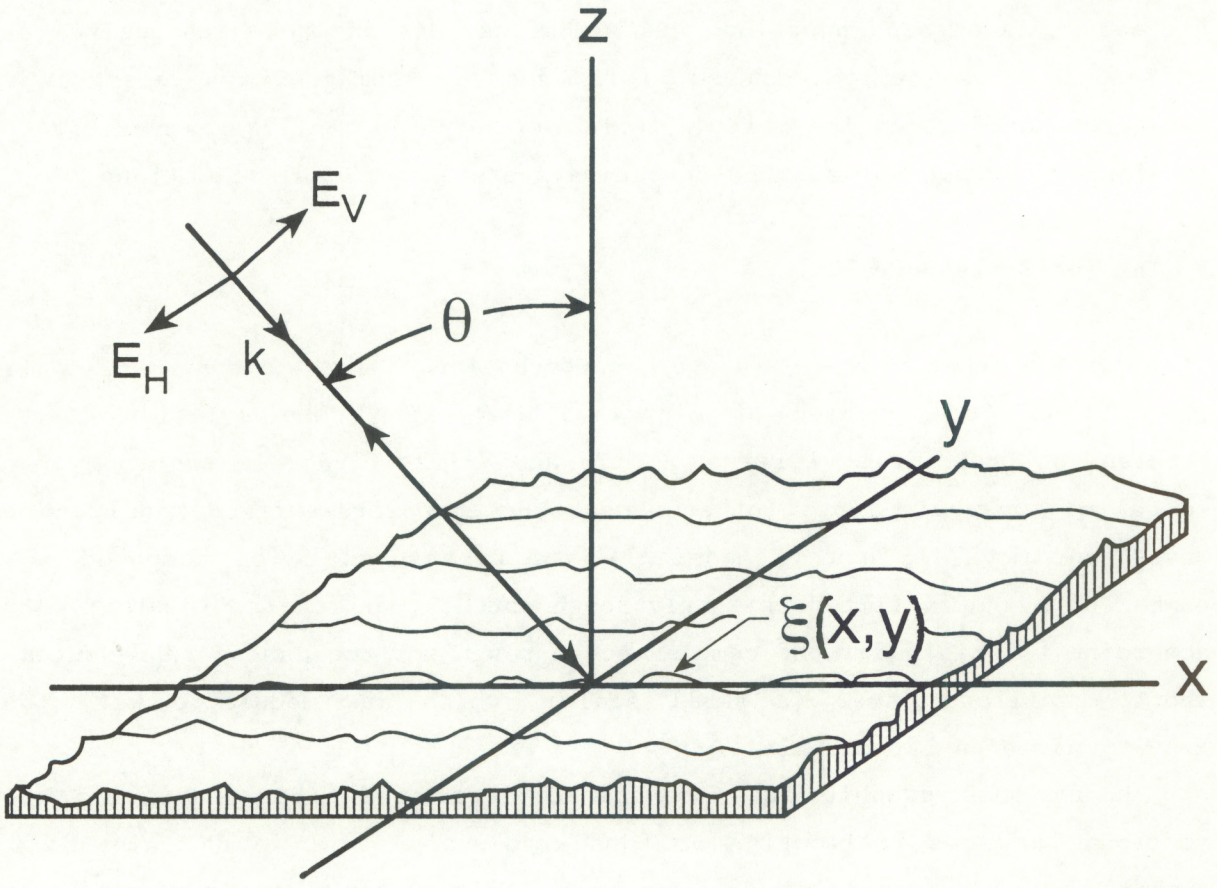

Figure 8. The scattering geometry.

(longer wavelengths) the sea surface can be considered as a perfectly conductive surface, $\epsilon \cong -i\infty$.

The presented equations can be applied very effectively for the case of HF wave scattering on the sea surface, because the sea wave heights are less than the electromagnetic wavelength in that case. For microwave scattering on the sea surface these equations are almost useless due to the opposite ratio of height to wavelength. Indeed, for these electromagnetic wavelengths the Bragg resonance condition will be fulfilled only for capillary waves, but not for longer surface waves, which are always present in real situations.

5. The Two-Scale Model

We see that Eqs.(1)-(4) of perturbation theory cannot be applied directly for the problem of microwave scattering. The solution to that problem was proposed by *Kuryanov* (1962) and *Wright* (1968) in the form of the so called two-scale model (other names: the composite-surface model and the wave-facet model). In this model the sea is assumed to be composed of an number of slightly tilted, slightly rough patches, or facets. In other words, according to this model the complex ocean rough surface can be represented as short, capillary waves (a small scale), which are modulated with long, gravity waves (a large scale).

Using this graphic idea, it is easy to derive backscattering cross sections for some realization of the large-scale wave. To do this, let us suppose from the beginning that we have a horizontal plane surface covered with only short, capillary waves, that the direction of wave incidence is situated in a vertical plane, and that the angle of incidence is ϑ. Then, assume that due to the passage of, say, long gravity waves, the normal to the surface in each point starts to deviate from the vertical direction by the angle ψ in the incidence plane, and by the angle δ in the plane perpendicular to the incidence plane. The resultant angle of incidence appears to be

$$\vartheta_i = \cos^{-1}[\cos(\vartheta + \psi)\cos\delta].$$

If we take into account this new angle of incidence in the equations of perturbation theory, the backscattering cross section per unit area for this

tilt-modulated surface takes the form, for horizontal polarization,

$$\sigma_{HH}(\vartheta_i) = 4\pi k^4 \cos^4\vartheta_i \left| \left(\frac{\alpha\cos\delta}{\alpha_i}\right)^2 g_{HH}^{(1)}(\vartheta_i) + \left(\frac{\sin\delta}{\alpha_i}\right)^2 g_{VV}^{(1)}(\vartheta_i) \right|^2 \times W(2k\alpha,\ 2k\gamma\sin\delta), \tag{5}$$

and for vertical polarization,

$$\sigma_{VV}(\vartheta_i) = 4\pi k^4 \cos^4\vartheta_i \left| \left(\frac{\alpha\cos\delta}{\alpha_i}\right)^2 g_{VV}^{(1)}(\vartheta_i) + \left(\frac{\sin\delta}{\alpha_i}\right)^2 g_{HH}^{(1)}(\vartheta_i) \right|^2 \times W(2k\alpha,\ 2k\gamma\sin\delta), \tag{6}$$

where $\alpha_i = \sin\vartheta_i$, $\alpha = \sin(\vartheta + \psi)$, $\gamma = \cos(\vartheta + \psi)$, and $g_{VV}^{(1)}$, $g_{HH}^{(1)}$ are the first-order scattering coefficients (3) and (4) (see, e.g., *Valenzuela*, 1978).

The further utilization of Eqs. (5) and (6) depends on the problem formulation. The angles ψ and δ describe the large-scale wave. If the shape of this wave is deterministic, the main problem is solved already. If the large-scale wave is stochastic, than additional calculation of averaged σ, or of its stochastic moments, over random ψ and δ is required. Keeping in mind the radar images from Fig. 6, we should obtain the corresponding σ for each pixel of an image by additional spatial averaging over an area of 30×30 m^2. Presumably one can assume the applicability of the ergodicity theorem for an ocean surface and change the spatial averaging to an ensemble averaging over tilts for waves with $\lambda_s < 30$ m. In principle, this can be done if we know the corresponding probability density functions for tilts. But examination of Eqs. (5) and (6) shows that the functional dependencies of σ_{HH} and σ_{VV} over ψ and δ are rather smooth and similar, and additional averaging cannot change the global behavior of the backscattering signal of different polarizations described by Eqs. (5) and (6).

Comparison of measured and theoretical cross sections of the ocean for a radar wavelength $\lambda = 6.7$ cm and two polarizations is presented in Fig. 9. In the next section we consider how the two-scale model can be incorporated into radar imaging theory, based on modulation transfer functions.

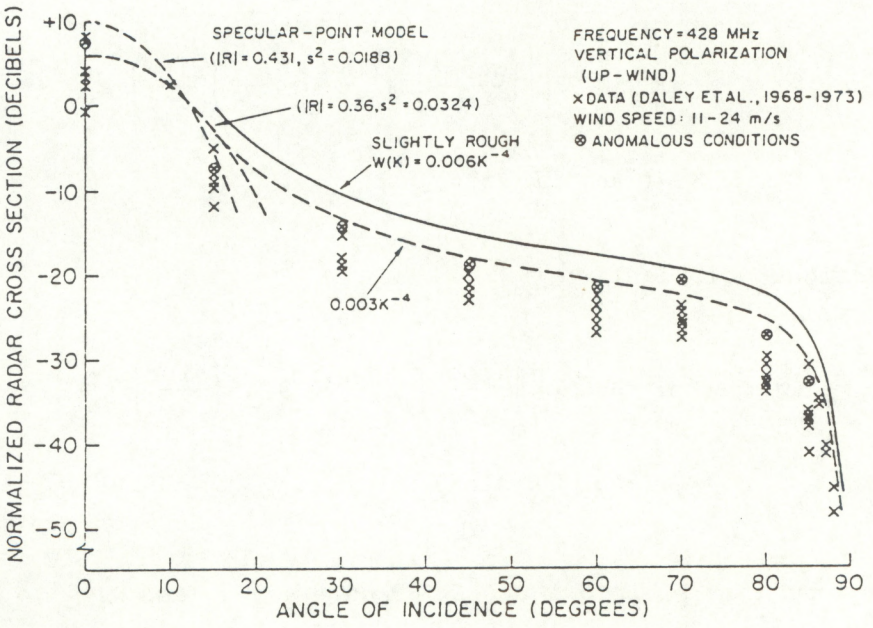

(a)

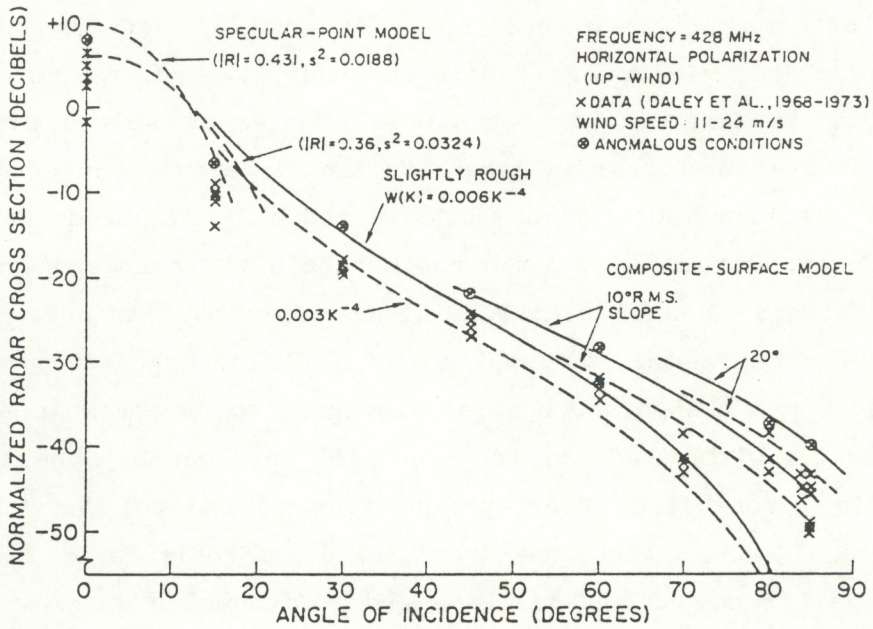

(b)

Figure 9. Comparison of measured and theoretical cross sections of the ocean for a radar wavelength λ = 6.7 cm: (a) *VV* polarization; (b) *HH* polarization (*Valenzuela*, 1978).

6. Two-Scale Model: Imaging of Sea Waves by Real-Aperture Radar

The two-scale model was used by *Keller and Wright* (1975), *Alpers and Hasselmann* (1978), and *Alpers et al.* (1981) for developing the so-called linear modulation theory for describing the imaging of ocean surface waves by real-aperture radar (RAR). For this purpose they introduced a modulation transfer function $R(\hat{\mathbf{k}})$, which is defined by

$$\sigma = \sigma_0 + \delta\sigma = \sigma_0\left[1 + \int \left(R(\hat{\mathbf{k}})Z(\hat{\mathbf{k}})\exp(i\hat{\mathbf{k}}\mathbf{r} - i\omega t) + \text{c.c.}\right)d\hat{\mathbf{k}}\right], \tag{7}$$

where σ is the normalized radar cross section and $Z(\hat{\mathbf{k}})$ is the Fourier transform of the surface elevation $\zeta(\mathbf{r})$ associated with the long waves.

$$\zeta(\mathbf{r}) = \iint\left(Z(\hat{\mathbf{k}})\exp[i(\hat{\mathbf{k}}\mathbf{r} - \hat{\omega}t)] + \text{c.c.}\right)d\hat{\mathbf{k}}, \tag{8}$$

where $\hat{\mathbf{k}}$ and $\hat{\omega}$ are the wave vector and radian frequency of the large-scale wave field, and c.c. stands for complex conjugate. The authors assume that the cross-section modulation depends linearly on the long wave field. This implies that $R(\hat{\mathbf{k}})$ does not depend on $Z(\hat{\mathbf{k}})$, which can be proved for low to moderate sea states.

The complex modulation transfer function (MTF) R is a sum of two terms, one that describes the hydrodynamic modulation, say, due to the interaction between short waves and long waves, and the other that is responsible for the tilt modulation:

$$R = R^{\text{hydr}} + R^{\text{tilt}} \tag{9}$$

The hydrodynamic contribution of the cross-section modulation is characterized by a nonuniform distribution of the short waves with respect to the long ocean wave field. According to perturbation theory this mechanism should affect both polarizations more or less in a similar manner, and this cannot help us with interpretation of Fig. 6. The tilt modulation is due to the purely geometric effect that Bragg scattering waves are seen by the radar at different local incidence angles depending on their location on the long wave. R^{tilt} can be easily calculated in the two-scale model presented above. It is convenient to represent the MTF as the sum of the longitudinal and

transverse parts:

$$R^{tilt} = R_{\parallel} + R_{\perp}, \tag{10}$$

where

$$R_{\parallel} = \frac{1}{\sigma_0} \frac{\partial \sigma}{\partial \psi}\bigg|_{\psi=0} i\hat{k}_{\parallel}, \qquad R_{\perp} = \frac{1}{\sigma_0} \frac{\partial \sigma}{\partial \delta}\bigg|_{\delta=0} i\hat{k}_{\perp}. \tag{11}$$

and $\hat{\mathbf{k}}_{\parallel}$ and $\hat{\mathbf{k}}_{\perp}$ are the components of the wave vector of the long wave in and perpendicular to the look direction of the antenna, respectively. In Fig. 10 one can see the calculated result of Eq. (11) for λ = 3 cm as a function of incidence angle for *HH* and *VV* polarizations. From curves in Fig. 10 it follows that the tilt modulation is larger for HH polarization than for VV polarization, although the cross section itself is smaller for HH polarization than for VV polarization.

If we assume that the theory is applicable for conditions that took place in the experiment by *A.V. Smirnov* (private communication, 1991), then (*a*) the radar image in Fig. 6*a* must be less bright that the image in Fig. 6*b*; and (*b*) the radar image in Fig. 6*a* must almost repeat but with a larger contrast, the pattern of the image in Fig. 6*b*. The first conclusion is qualitatively true, but the second conclusion is absolutely wrong. Thus, we may conclude that the two-scale Bragg model cannot explain the polarization peculiarities seen in Fig. 6.

7. New Models and New Approaches

We can find much evidence in the literature that the two-scale model is not satisfactory in many cases. Strong criticism of this theory is increasing with accumulation of new experimental data (see, e.g., *Pierson*, 1990). As noted above, the discrepancy between the two-scale calculations of the polarized radar return and measured values arises for small grazing angles and developed sea states. *Kalmykov and Pustovoytenko* (1976) observed such a discrepancy under the same conditions. They explained this by the presence of "wedge" scattering.

The analysis of scatterometer data of *Donelan and Pierson* (1987) shows

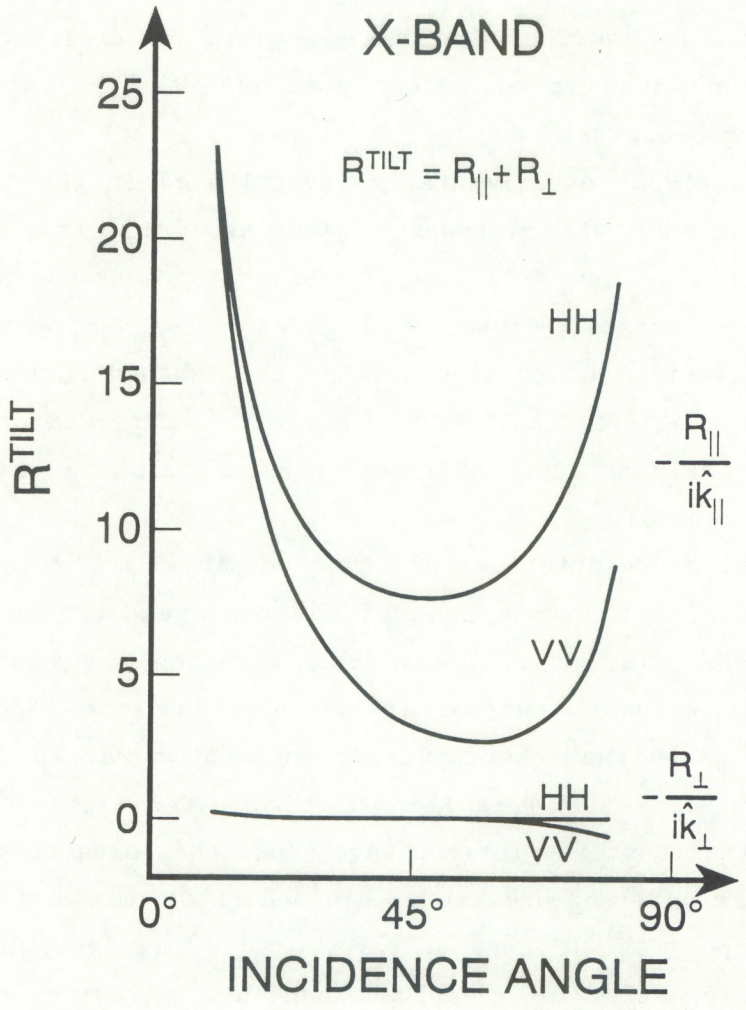

Figure 10. Dimensionless tilt modulation transfer function (R^{tilt}) as a function of incidence angle for *HH* and *VV* polarizations in *X*-band (*Alpers et al.*, 1981).

that for small grazing angles and high winds, the two-scale Bragg model yields values that are sufficiently different compared with the data for *HH* and *VV* polarizations. Figure 11 shows their measured versus calculated ratios of horizontally polarized to vertically polarized backscatter for upwind and downwind conditions for various incidence angles. An explanation of these results was offered in terms of recent popular ideas of backscatter from wedges and spilling breakers.

Kwoh and Lake (1984) experimentally investigated in the laboratory the fundamental mechanisms of microwave backscattering from mechanically generated short gravity waves. It was found that microwave backscattering occurs in discrete bursts which are highly correlated with the gentle breaking of waves. Using numerical modeling, they showed that for a wave in the process of breaking, its small-radius crest is the predominant scattering source in a manner akin to wedge diffraction as described by the geometrical theory of diffraction (GTD).

A comprehensive description of the possible mechanisms for such non-Bragg scattering, but in the case of the real sea surface, was done by *Wetzel* (1986, 1990). His basic object is a breaking wave, or breaker. He noted that breaking waves occurring in the open sea are generally of the spilling type, in which the interior crest angle at a wave peak sharpens to the point of instability (120^0), and a series of water masses emitted at the crest slide down the front face of the wave under the force of gravity. Along the crest line this spilling breaker is divided on "plumes." The plume has a characteristic shape (Fig. 12) and entrains air to form the whitecap. It is clear that scattering effect of the plumes can only be seen by radar when the radar is looking upwind, because of geometrical considerations.

It should be note that it is very difficult to combine this morphological approach with statistical scattering theory. The author does not even attempt this. He treats the breaker as a single target, so a cross section of the target is computed for different polarizations. Unfortunately, there is little reliable experimental evidence available that could either confirm or deny this scattering hypothesis.

Nevertheless, if we include into our considerations such a new scattering object as a plume, we have more possibilities for modeling different polarization-dependent phenomena. First, because of grazing

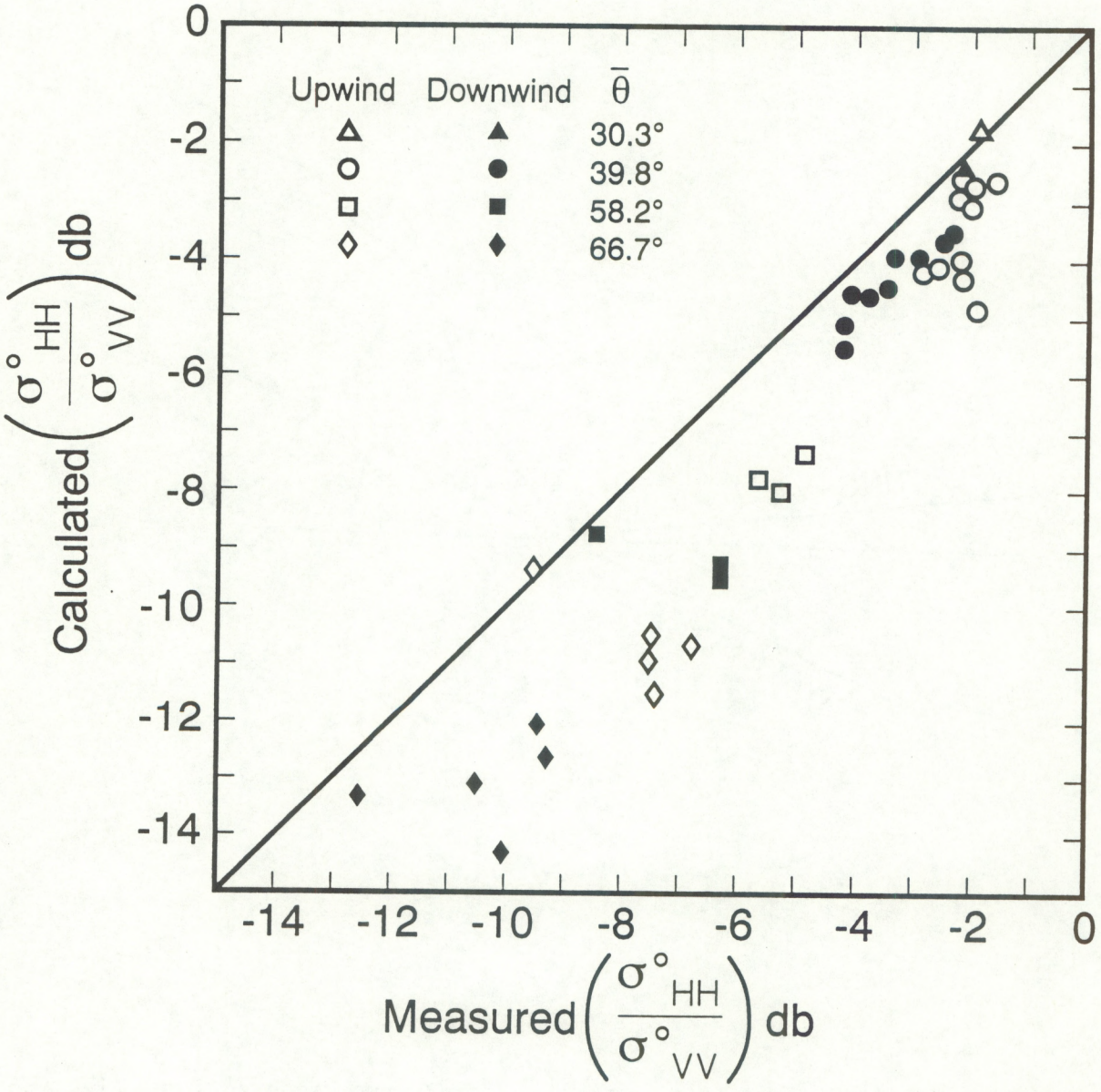

Figure 11. Measured versus calculated ratio of horizontally polarized to vertically polarized backscatter for upwind and downwind conditions for various incidence angles (*Donelan and Pierson*, 1987).

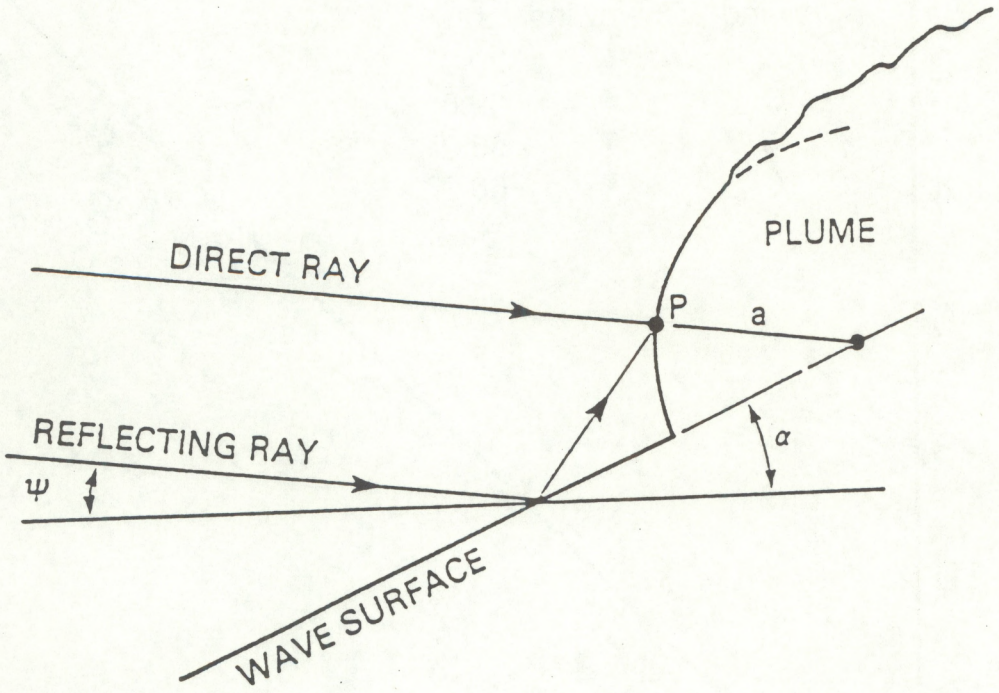

Figure 12. Geometry for simple wave-surface/plume interactions (*Wetzel*, 1990).

propagation the back specular reflection from breakers can play an important role. Second, as proposed by *Wetzel* (1990), double scattering may occur in the vicinity of the toe of the breaker. His argument is the following. When the circumference of the segment in Fig. 12 is long compared to a wavelength ($ka \gg 1$), it is appropriate to use the physical optics (Kirchhoff) approximation. Here the scattering takes place at the point of specular reflection, shown as the point P in Fig. 12. However, the water surface ahead of the scatterer produces a reflected wave that must be added to the incident wave in the neighborhood of P. Strictly speaking, for very large ka, the surface-reflected wave will itself be specularly reflected at P, away from the incident direction. However, for relatively small values of grazing angle ψ, and modest values of ka, the scattering patterns of the direct and surface-reflected waves at P should overlap back at the source. The effect may be simulated by multiplying the specular-point cross section by an angle-and-polarization-dependent factor based on the geometry of Fig. 12:

$$F^2 = \left| E_{direct} + E_{reflected} \right|^2$$

$$F^2_{V,H}(a,f,\psi) = \left| \exp(ika\cos 2\psi) + R_{V,H}(f,\psi)\exp(ika) \right|^2, \qquad (12)$$

where $R_{V,H}(f,\psi)$ is the (complex) reflection coefficient for an incident wave of frequency f and grazing angle ψ. We call F^2 the surface proximity function. It is plotted for both polarizations, in Fig. 13*a* for ka = 2, 4, 6 and in Fig. 13*b* for the larger values ka = 10, 20.

It should be noted here that the picture of this double-scattering consideration is not complete without including the effects of enhanced backscattering. Wetzel has considered only one possible trajectory for the double-scattered wave. But there exists the second, backward trajectory that must be taken into account. It becomes obvious if we reverse the direction of the wave shown in Fig. 12. Therefore, we have to add coherently the complex amplitudes of the wave considered by Wetzel and of the backward wave. In that case we have a problem similar to the one considered in the works of *Mendez and O'Donnell* (1987), *O'Donnell and Knotts* (1991), and *Soto-Crespo and*

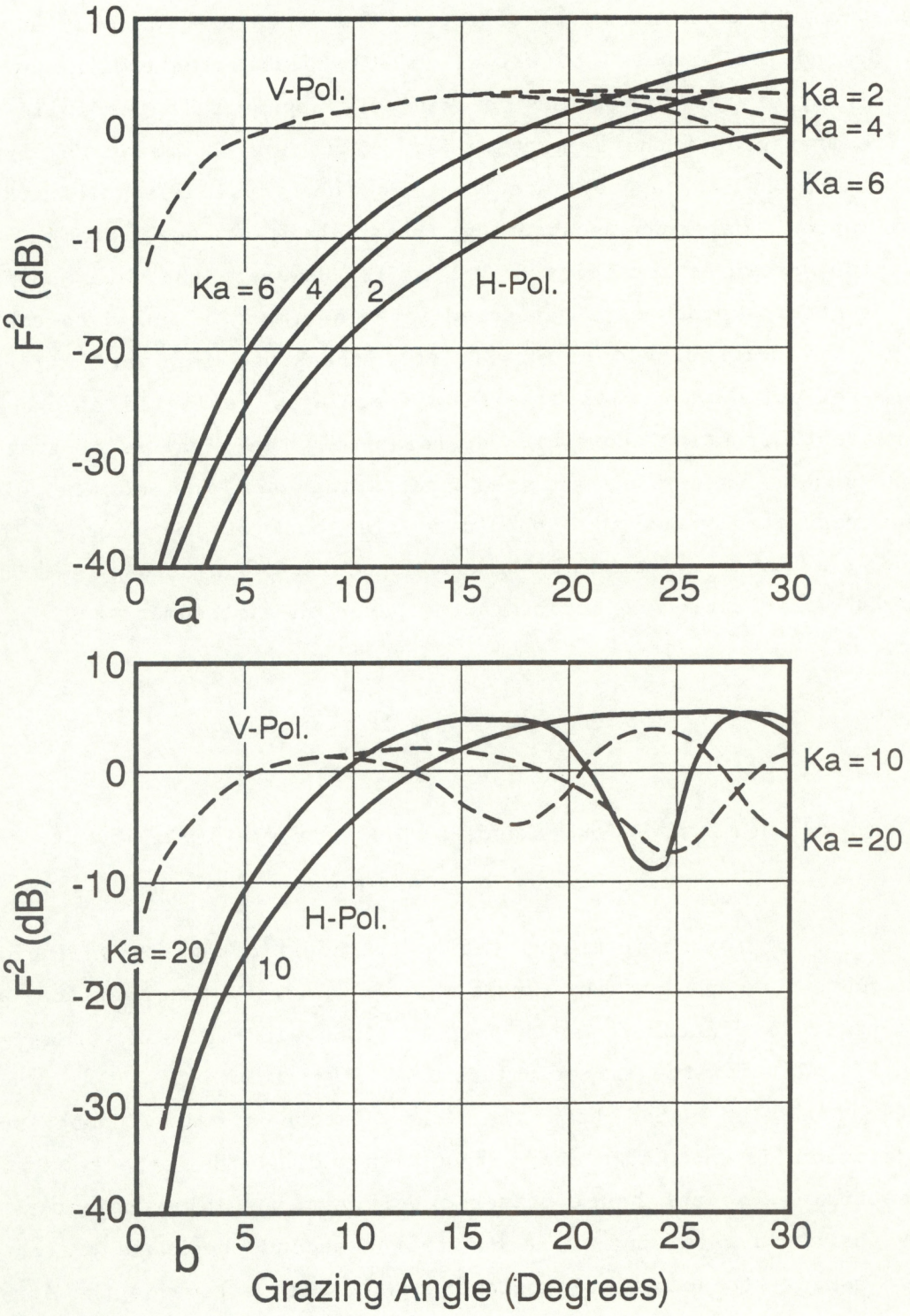

Figure 13. The surface proximity factor $F^2_{V,H}(a,f,\psi)$ (*Wetzel*, 1990):(a) *ka* = 2,4, and 6; (b) *ka* = 10 and 20.

Nieto-Vesperinas (1989). These authors have found experimentally and numerically that the effect of enhanced backscattering for solid conducting surfaces is accompanied by a strong depolarization effect. But, to our knowledge, no one considered electromagnetic scattering on the ocean surface under this aspect.

We see that the new approaches mentioned above are closely related to the new feature noted in the polarization behavior of the radar return, but they are meaningful only for sufficiently large angles of incidence (grazing scattering) and for a well-developed sea including breakers. As to the grazing-angle geometry, it takes place only for the more distant areas in the presented radar images. The winds near the exposed surface were pretty weak, according to *A.V. Smirnov* (private communication, 1991). This means that other models for the ocean waves should be examined.

8. Conclusions

(a) Attempts to explain the differences in the radar pictures using *HH* and *VV* polarizations run into severe problems because of electromagnetic scattering from the *real sea*.

(b) We have shown that these images cannot be explained using the two-scale Bragg model.

(c) New approaches represent only a collection of physical mechanisms that should be combined in a more consistent way. A robust theory is desirable.

(d) We need additional qualitative information about the radar images. Part of this information can be extracted from the existing images after spectral and statistical processing.

9. References

Alpers, W., and K. Hasselmann, 1978, The two-frequency microwave technique for measuring ocean wave spectra from an airplane or satellite, *Boundary Layer Meteorol.*, 13, 215-230.

Alpers, W.R., D.B. Ross, and C.L. Rufenach, 1981, On the detectability of

ocean surface waves by real and synthetic aperture radar, *J. Geophys. Res.*, **86**, No.C7, 6481-6498.

Barrick, D.E., 1972, Remote sensing of sea state by radar. in *Remote Sensing of the Troposphere*, V.E. Derr (ed.), NOAA Environmental Research Laboratories, Boulder, CO, 12-1 - 12-34.

Bass, F.G., and I.M. Fuks. 1979, *Wave Scattering from Statistically Rough Surfaces*. International Series in Natural Philosophy, v.93. C.B. Vesecky and J.F. Vesecky (eds.), Pergamon Press, Oxford. (Russian original edition: 1972.)

Beckmann, P., and A. Spizzichino, 1963, *The Scattering of Electromagnetic Waves from Rough Surfaces*, Pergamon Press, Oxford.

Bravo-Zhivotovskiy, D.M., N.I. Volodina, L.B. Gordeev, A.M. Dronov, Yu.M. Zhidko, E.M. Zuykova, A.G. Luchinin, S.A. Maryutin, S.I. Muyakshin, Ye. N. Pelinovskiy, A.M. Sutin, V.I. Titov, and Yu. B. Shchegol'kov, 1982, Remote sensing of the effect of internal waves on the surface wave in the ocean, *Dokl. Akad. Nauk SSSR*, **265**, 457-460.

Donelan, M.A., and W.J. Pierson, Jr. 1987, Radar scattering and equilibrium ranges in wind-generated waves with application to scatterometry, *J. Geophys. Res.*, **92**, 4971-5029.

Etkin, V.S., M.D. Raev, M.G. Bulatov, Yu. A. Militsky, A.V., V. Raizer, Yu. A. Trokhimovsky, V.G. Irisov, A.V. Kuzmin, K. Ts. Litovchenko, E.A. Bespalova, E.I. Skvortsov, M.N. Pospelov, A.I. Smirnov, 1991, *Radiohydrophysical Aerospace Research of an Ocean*. Preprint of Space Research Institute, USSR Academy of Sciences, Moscow, 84 pp.

Hughes, B.A., and H.L. Grant, 1978, The effect of internal waves on surface wind waves, 1, Experimental measurements, *J. Geophys. Res.*, **83**, 443-454.

Kalmykov, A.I., and V.V. Pustovoytenko, 1976, On polarization features of

radio signals scattered from the sea surface at small grazing angles, *J. Geophys. Res.*, **81**, 1960-1964.

Keller, W.C. and J.W. Wright, 1975, Microwave scattering and straining of wind generated waves, *Radio Sci.*, **10**, 139-147.

Kinsman, B., 1965, *Wind Waves: Their Generation and Propagation on the Ocean Surface*, Prentice Hall, Englewood Cliffs, NJ. (Reprinted by Dover, New York, 1984.)

Kuryanov, B.F., 1962, The scattering of sound on the rough surface with two types of roughness, *Akust. Zh.*, **10**, 325 (In Russian.)

Kwoh, D.S.W., and B.M. Lake, 1984, Deterministic, coherent, and dual-polarized laboratory study of microwave backscatter from water waves, I, Short gravity waves without wind, *IEEE J. Oceanic Eng.*, **OE-9**(5), 291-308.

Lavrova, O.Yu., A.D. Rosenberg, and A.V. Smirnov, 1991, Measurement of the spatial spectra of a disturbance using aircraft side-looking radar, *Sov. J. Remote Sensing*, **9**(3), 374-390.

Mendez, E.R., and K.A. O'Donnell, 1987, Observation of depolarization and backscattering enhancement in light scattering from Gaussian random surfaces, *Opt. Commun.*, **61**, 91-95.

Mityagina, M.I., V.G. Pungin, A.V. Smirnov, and V.S. Etkin, 1991, The changes in the power-carrying part of sea surface wave spectrum in a field of internal wave according to remote observation, *Izves. Atmos. Ocean. Phys.*, **27**, 925-929.

O'Donnell, K.A., and M.E. Knotts, 1991, The role of polarization in enhanced backscattering from rough surfaces, in *Proceedings of ICO Topical Meeting on Atmospheric, Volume and Surface Scattering and Propagation*, Florence, Italy, August 27-30, 1991, 231-234.

Peak, W.H., 1959, Theory of radar return from terrain, *IRE Natl. Conv. Rec.*, **7**, 27-41.

Pierson, W.J., Jr., 1990, Dependence of radar backscatter on environmental parameters, in *Surface Waves and Fluxes*, Volume II - Remote Sensing, G.L. Geernaert and W.L. Plant (eds.), Kluwer Academic Publishers, Dordrecht, 173-220.

Scolnik, M.I., 1968, Sea echo, in *Radar Handbook*, M.I. Scolnik (ed.) 26-1 - 26-30.

Soto-Crespo, J.M., and M. Nieto-Vesperinas, 1989, Electromagnetic scattering from very rough random surfaces and deep reflection gratings, *J. Opt. Soc. Am.*, **A6**, 367-384.

Valenzuela, G.R., 1978, Theories for the interaction of electromagnetic and oceanic waves -- A review, *Boundary Layer Meteorol.*, **13**, 61-85.

Wetzel, L.B., 1986, On microwave scattering by breaking waves, in *Wave Dynamics and Radio Probing of the Ocean Surface*, O.M. Phillips and K. Hasselmann (eds.), Plenum, New York, 273-284.

Wetzel, L.B., 1990, Electromagnetic scattering from the sea at low, grazing angles, in *Surface Waves and Fluxes*, Volume II - Remote Sensing, G.L. Geernaert and W.L. Plant (eds.), Kluwer Academic Publishers, Dordrecht, 109-171.

Wright, J.W., 1966, Backscattering from capillary waves with application to sea clutter, *IEEE Trans. Antennas Propag.*, **AP-14**, 749-754.

Wright, J.W., 1968, A new model for sea clatter, *IEEE Trans. Antennas Propag.*, **AP-16**, 217-223

Zebker, H.A., and J.J. Van Zyl, 1991, Imaging radar polarimetry: A review, *Proc. IEEE*, **79**, 1583-1606. *U.S. GOVERNMENT PRINTING OFFICE: 1993-774-025/69050